Journal of Biomedical Optics 8(3), 472–478 (July 2003)

Metal-enhanced emission from indocyanine green: a new approach to *in vivo* imaging

Joanna Malicka
Ignacy Gryczynski
University of Maryland School of Medicine
Department of Biochemistry & Molecular Biology
Center for Fluorescence Spectroscopy
725 W. Lombard Street
Baltimore, Maryland 21201-1503

Chris D. Geddes
University of Maryland Biotechnology Institute
725 W. Lombard Street
Baltimore, Maryland 21201-1503

Joseph R. Lakowicz
University of Maryland School of Medicine
Department of Biochemistry & Molecular Biology
Center for Fluorescence Spectroscopy
725 W. Lombard Street
Baltimore, Maryland 21201-1503
E-mail: lakowicz@cfs.umbi.umd.edu

Abstract. Indocyanine green (ICG) is widely used in medical imaging and testing. Its complex spectral behavior and low quantum yield limits some applications. We show that proximity of ICG to a metallic silver particle increases its intensity approximately 20-fold and decreases the decay time. Since the rate of photobleaching is not increased, our results suggest that ICG-silver particle complexes can yield at least 20-fold more photons per ICG molecule for improved medical imaging. [DOI: 10.1117/1.1578643]

Keywords: metal-enhanced fluorescence; idocyanine green; silver islands.

Paper JBO 02050 received Jul. 30, 2002; revised manuscript received Jan. 15, 2003 and Feb. 25, 2003; accepted for publication Mar. 3, 2003.

1 Introduction

Indocyanine green (ICG) is a tricarbocyanine dye (Scheme I) with near-infrared (NIR) absorption and emission maxima near 780 and 820 nm, respectively. In addition, ICG is not toxic and is approved by the U.S. Food and Drug Administration for use in humans, typically by injection. ICG has a large number of medical applications, including retinal angiography[1,2]; measurement of plasma volume,[3] cardiac output,[4] and photocoagulation[5]; assessment of burn depth,[6] liver function,[7] and exercise physiology[8]; and guiding biopsies.[9] ICG is also being investigated for other uses such as optical tomography[10–11] and optical tumor detection.[12]

ICG displays complex associative and spectral properties in solution,[13–15] resulting in attempts to normalize the spectral properties and improve stability.[16,17] These attempts rely on binding ICG to proteins, micelles, or membranes, or binding to charged polymers. We now describe an alternative approach to improving the stability and brightness of ICG. Our approach makes use of the improved solubility and spectral properties of ICG when it is bound to albumin, but in addition makes use of a physical interaction of ICG with metallic silver particles.

In recent publications we described the effects of silver particles on a number of fluorophores.[18–21] We found that proximity to the metallic surfaces resulted in increased intensities, decreased lifetimes, and moderate increases in photostability. These effects occur because the excited fluorophores interact with freely mobile electrons in the metal, resulting in increased rates of radiative decay. These interactions with the surface plasmons are complex. They have been the subject of theoretical analysis and are closely related to surface-enhanced Raman spectroscopy (SERS).[22–24] We have recently described the use of metal–fluorophore interactions as radiative decay engineering.[18,19]

Here we report on a study of ICG bound to human serum albumin (HSA), which in turn was bound to unsilvered or silvered surfaces. The silvered surfaces were silver island films (SIFs), which consist of a noncontinuous coating of silver particles on a glass substrate deposited by chemical reduction of silver.[25] The quartz and quartz-SIF surfaces were coated with HSA, which is known to passively adsorb to such surfaces,[26] allowing us to study the fluorescent spectral properties of noncovalent ICG-HSA complexes in the absence and presence of the silver particles.

2 Materials and Methods

ICG was obtained from Sigma Chemical Co. ICG bound to HSA was prepared by mixing an aqueous solution of ICG with a solution of HSA to a final concentration of 30 μM ICG and 60 μM HSA. Immediately upon mixing, the absorption spectrum of ICG changed from the aggregate spectra with two absorption maxima near 700 and 780 nm to the monomer spectrum with an absorption maximum near 795 nm. Concentrations were determined using $\epsilon(780\ \text{nm}) = 130{,}000\ \text{M}^{-1}\text{cm}^{-1}$ for ICG and $\epsilon(278\ \text{nm}) = 37{,}000\ \text{M}^{-1}\text{cm}^{-1}$ for HSA. Binding to the surface was accomplished by soaking both the quartz and the SIF slides in the ICG-HSA solution overnight, followed by rinsing with water.

2.1 *Silver Island Films*

Silver island films were formed on quartz microscope slides according to published procedures,[25] as modified in our recent reports.[19] This procedure consists of reducing silver nitrate with D-glucose under controlled conditions.[19] This results in a partial coating of the quartz with silver islands (Fig. 1, bottom left). The diameters of the islands are from 100 to 500 nm across and near 60 nm high, with some aggregates. These particles display a characteristic surface plasmon resonance

Chemical structure of ICG.

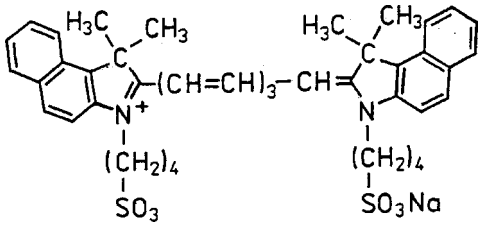

with a maximum near 480 nm that is characteristic of silver particles, and an optical density near 0.2 (Fig. 1, bottom right).

2.2 *Geometry of the Sample*

Our sample configuration is shown in Fig. 1 (top). Half of the slide was covered with SIFs. The albumin-coated surface, with and without SIFs, was covered with the other side of a demountable cuvette, with water between the surfaces.

2.3 *Fluorescence Measurements*

Emission spectra were obtained using a Spectra Physics Tsunami titanium:sapphire (Ti:S) laser in the continuous wave (c.w.) (nonpulsed) mode with output at 765 nm. The emission spectra were recorded through a long-pass filter from Edmund Scientific that cut off wavelengths below 780 nm. Intensity decays were measured in the time domain using 750-nm excitation from a mode-locked argon ion pump, cavity-dumped pyridine 2 dye laser with a 3.77-MHz repetition rate. Time-correlated single-photon counting (TCSPC) was accomplished using an SPC630 PC card from Becker & Hickl GmbH, in reverse start-stop mode, and a microchannel plate photomultiplier tube (PMT). The instrumental response function, determined with the sample geometry (Fig. 1) and a scattering sample was typically <30 ps FWHM. The data were analyzed using nonlinear least-squares impulse reconvolution with a goodness of fit, χ^2_R, criterion. For lifetime measurements we used the long-pass filter with an additional 830-nm interference filter to alleviate scattered light. All measurements were performed using front-face geometry in a 0.1-mm demountable cuvette or between quartz slides, with vertically polarized excitation and fluorescence emission observed at the magic angle, 54.7°. Frequency-domain measurements[27] were performed using 700-nm excitation, 7-ps pulses at 7.6 MHz, from a pyridine 1 dye laser. This instrument has an upper frequency limit of 10 GHz and is capable of measuring decay times of just several picoseconds. The intensity decay data were analyzed in terms of the multiexponential model

$$I(t)=\sum_i \alpha_i \exp(-t/\tau_i), \tag{1}$$

where τ_i are the lifetimes with amplitudes α_i and $\Sigma\alpha_i=1.0$. The contribution of each component to the steady-state intensity is given by

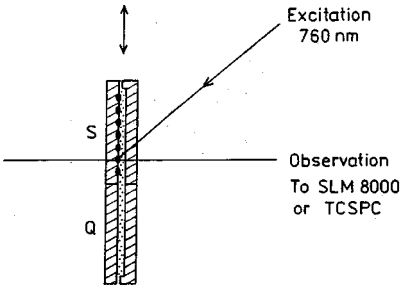

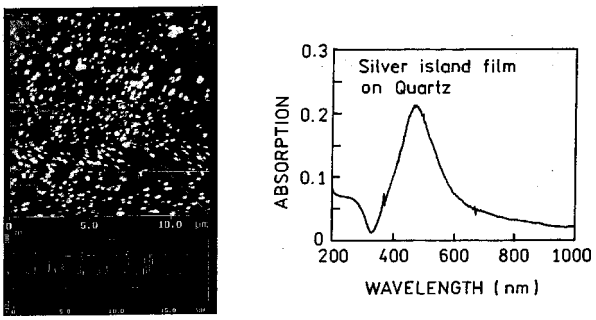

Fig. 1 Sample geometry (top), atomic force microscopy (AFM) image (bottom left) and absorption spectrum (bottom right) SLM8000-spectrofluorimeter.

$$f_i=\frac{\alpha_i\tau_i}{\sum_j \alpha_j\tau_j}. \tag{2}$$

The mean decay time is given by

$$\overline{\tau}=\sum_i f_i\tau_i. \tag{3}$$

The amplitude-weighted lifetime is given by

$$\langle\tau\rangle=\sum_i \alpha_i\tau_i. \tag{4}$$

3 Results

The emission spectra of ICG-HSA bound to quartz or SIFs are shown in Fig. 2. The intensity of ICG is increased approximately 20-fold on the SIFs compared with the unsilvered quartz surface (top). The emission spectrum was not detectably shifted by the silver particles (bottom). We found the same increase in ICG emission whether the surfaces were coated with HSA, which already contained bound ICG, or if the surfaces were first coated with HSA followed by exposure to a dilute aqueous solution of ICG. From ongoing studies of albumin-coated surfaces, we know that roughly the same amount of HSA binds to each surface, with the difference in binding being less than a factor of two.[28] Hence the intensity increase seen on the SIF is not due to increased ICG-HSA binding but rather to a change in the quantum yield and/or rate of excitation of ICG near the silver particles.

Fluorophores can have several interactions with metallic surfaces, including quenching, an increase in the rate of radiative decay, or an increased rate of excitation that is due to an

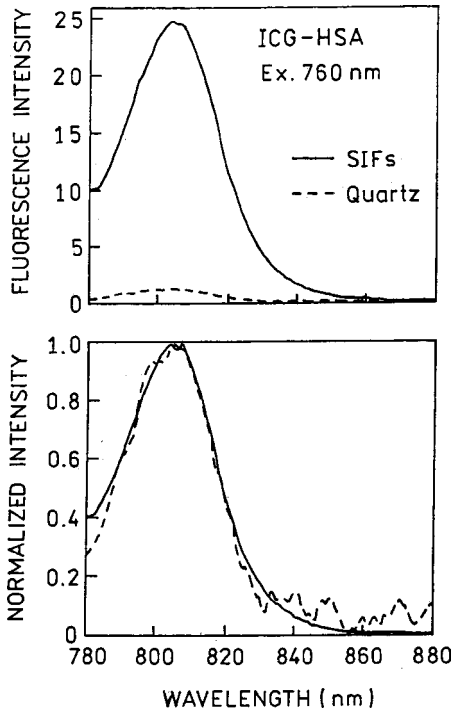

Fig. 2 Emission spectra of indocyanine green-albumin (ICG-HSA) bound to unsilvered quartz slides or silver island films. Top panels, as measured; bottom panel, peak normalized.

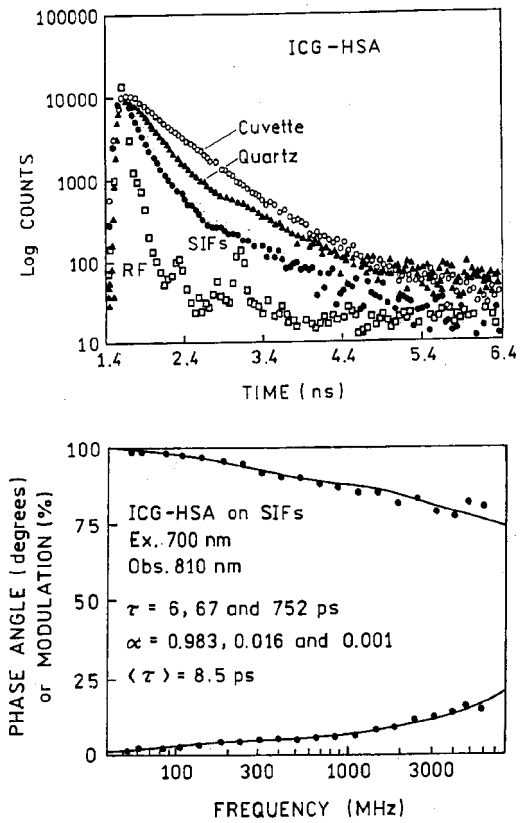

Fig. 3 Time-dependent intensity decays of ICG-HSA, top: time-domain data, bottom: frequency-domain data for ICG-HSA on silver.

increased excitation field. This last interaction is called the lightning rod effect. Lifetime measurements can distinguish among these interactions. The intensity will be higher because of the increased electric field around the metal particles.[24] Consider the usual definition of the lifetime (τ) and quantum yield (Q):

$$Q=\frac{\Gamma}{\Gamma+k_{\mathrm{nr}}} \tag{5}$$

$$\tau=\frac{1}{\Gamma+k_{\mathrm{nr}}}, \tag{6}$$

where Γ is the radiative decay rate and k_{nr} is the sum of the nonradiative decay rates. A quenching interaction will increase k_{nr} so that the quantum yields and lifetimes decrease in unison. An increased rate of excitation that is due to the lightning rod effect will not affect Γ or k_{nr}.

Unusual effects are expected if the radiative decay rate is increased from Γ to $\Gamma+\Gamma_m$ near the metal. Then the quantum yield and lifetimes are given by

$$Q=\frac{\Gamma+\Gamma_m}{\Gamma+\Gamma_m+k_{\mathrm{nr}}} \tag{7}$$

and

$$\tau=\frac{1}{\Gamma+\Gamma_m+k_{\mathrm{nr}}}. \tag{8}$$

An increase in the total radiative rate to $\Gamma+\Gamma_m$ results in an increased quantum yield and a decreased lifetime. We examined the intensity decay of ICG-HSA on quartz or SIFs (Fig. 3, top). The intensity decays much more rapidly when ICG-HSA is bound to the SIF compared with the quartz surface. When bound to SIFs, the intensity decay of ICG-HSA becomes dominated by a short decay time near 6 ps. Because of the rapid decay components seen in the time-domain data, we also examined the intensity decays with our 10-GHz frequency-domain instrument.[27] These measurements also show a dominant 6-ps component (Fig. 3, bottom). The similarity of the intensity decays measured in the time and frequency domain can be seen from the impulse response functions (Fig. 4). These functions also clarify that the visual difference between the cuvette and quartz is due to the effects of convolution of the impulse response function with the instrument response function. We attribute this component to a population of ICG molecules that are an appropriate distance from a silver surface to display an increased quantum yield and decreased lifetime. In recent studies we found that maximum enhancement was observed for fluorophores that were 40 to 90 Å from the silver surfaces.[28]

Examination of Table 1 reveals that the preexponential factor for the shortest decay time, presumably for ICG-HSA on SIFs, is 0.982. It is well known that for a fluorophore in two environments, with a different lifetime in each environment, the normalized α_i values represent the fraction of molecules present in each environment. This comparison gives the erroneous impression that 98% of the ICG-HSA molecules display enhanced fluorescence. However, the α_i values only represent the molecular fractions when the radiative decay rate is

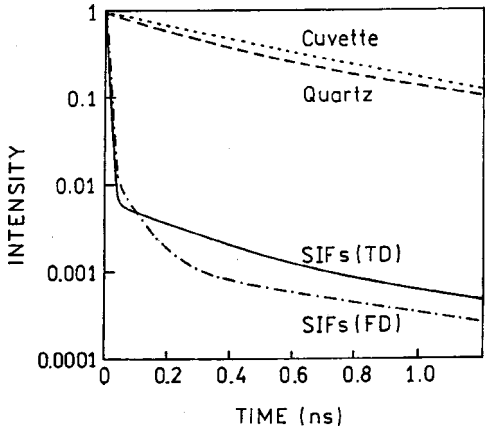

Fig. 4 Impulse response functions of ICG-HSA in buffer (cuvette), on quartz, and on silver island films (SiFs) (i.e., the αs and τs from Table 1, which were obtained from the convolution procedure).

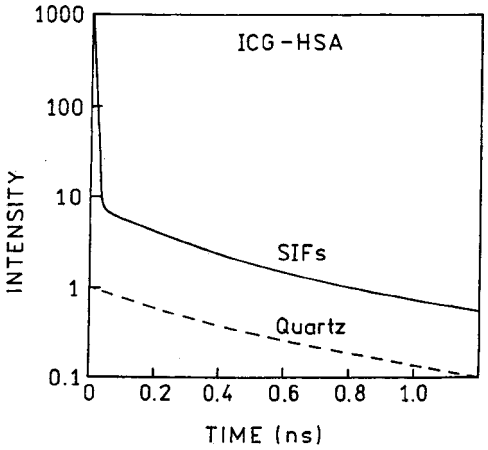

Fig. 5 Intensity decay of ICG-HSA with time-integrated areas normalized to the relative steady-state intensities (Fig. 2).

the same in each environment or for each lifetime component. If the radiative decay rate of a population is increased, as we believe occurs near SIFs, then the normalized α_i value for this population is larger than the molecular fraction near the SIFs. This concept is described in more detail in the appendix.

Additional insight can be gained by examining the intensity decays normalized so that the integrated area under the decay is equal to the relative steady-state intensities. This normalization is based on the fact that the time-integrated intensity decay, given by the $\Sigma \alpha_i \tau_i$ products, is proportional to the steady-state intensity (appendix). Figure 5 shows that the 6-ps component is a new component that appears without a significant decrease in the long-lived component. This result suggests to us that the 6-ps component is due to a small subpopulation of the ICG-HSA molecules that is at a distance from the metal which results in dramatically increased fluorescence. If this is true, then the signal from ICG could be enhanced to a greater extent using procedures that position a larger fraction of the ICG molecules near the silver surfaces.

ICG is known to rapidly degrade in solution as a result of chemical and/or photochemical processes. The 20-fold increase in intensity of ICG-HSA seen in Fig. 2 would not be useful if the sample degraded 20-fold more rapidly. We examined the steady-state intensity of ICG-HSA with continuous illumination. Upon initial exposure, the relative intensity of ICG-HSA decays more rapidly on SIFs than on quartz (Fig. 6, top). However, the effect is modest and the photobleaching rates become comparable after 1 min. If the illumination intensity is adjusted to yield the same intensity at the start of illumination, the ICG-HSA on SIFs photobleaches somewhat slower (Fig. 6, bottom). The detectable signal from the ICG-BSA is given by the area under these photobleaching curves, demonstrating that prior to photobleaching, about 20-fold more emission can be obtained on SIFs than on quartz. This increased signal might be larger if the measurements were extended to longer times. It is important that the ICG intensity near SIFs remains higher even after the initial decrease in intensity (Fig. 6, top), which suggests that ICG will display higher intensities for longer times when it is bound near silver particles.

Table 1 Multiexponential intensity decay of ICG-HSA.

Sample[a]	α_i	τ_i (ns)	f_i	$\bar{\tau}$ (ns)	$\langle\tau\rangle$ (ns)	χ^2_R
In water, TD	0.158	0.190	0.05	—	—	
	0.842	0.615	0.95	0.592	0.548	1.4
On quartz, TD	0.558	0.233	0.272	—	—	
	0.442	0.792	0.728	0.645	0.484	1.4
On SIFs, TD	0.993	0.006	0.705	—	—	
	0.005	0.215	0.127	—	—	
	0.002	0.799	0.168	0.151	0.008	1.4
On SIFs, FD	0.982	0.006	0.756	—	—	
	0.016	0.067	0.130	—	—	
	0.001	0.752	0.114	0.099	0.008	1.8

[a] TD, time domain; FD, frequency domain.

4 Discussion

We questioned whether it was practical to consider metallic particles for medical applications. For purposes of injection it would be necessary to use colloidal suspensions of the metal rather than SIFs. It appears that colloidal silver is deemed safe because it has been used for topical applications, as an antibiotic, and ingested orally to aid in cessation of smoking.[29,30] Sublingual applications of colloidal silver result in rapid transport into the bloodstream.[31] Gold is used as an injectable suspension for treatment of arthritis.[32] While particulates may seem unsuitable for injection, there are many ongoing studies on using polymeric particles to deliver protein and drugs[33,34] or magnetic resonance imaging (MRI) contrast agents.[35,36] However, we were unable to find literature describing the use and/or toxicity of injected silver colloids.

Another significant opportunity is the combined use of enhanced fluorescence and the scattering properties of metallic

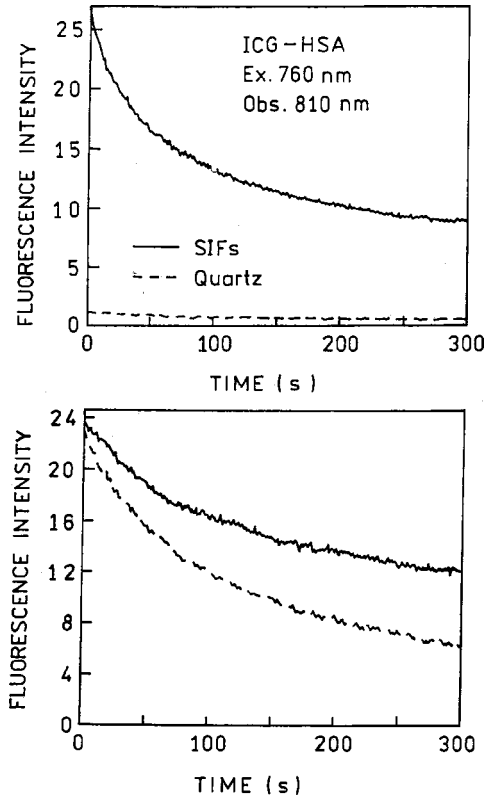

Fig. 6 Photostability of ICG-HSA on quartz and on SIFs, measured with the same excitation power (top) and with adjusted power to provide the same initial fluorescence intensity (bottom).

colloids. The surface plasmon of colloidal silver, gold, and some other metals results in high cross-sections for light scattering.[37,38] The strong scattering makes it easy to detect low concentrations of particles.[39] One could use both the strong scattering and enhanced fluorescence for improved detection in tissues. Alternatively, the metal colloids may be derivatized with sensing fluorophores, such as those sensitive to pH or cations. In this case the scattering can be used to locate the colloids, and the fluorophore emission used to determine the local concentration of analytes.

Appendix: Multiexponential and Metal-Enhanced Intensity Decays

Multiexponential Intensity Decays

The intensity decays of fluorophores near metallic particles display unique features not encountered in typical multiexponential decays. This difference can be seen by a close examination of the decay parameters, with careful definition of the parameters. First consider a fluorophore that displays a single exponential decay:

$$I(t)=k\Gamma N(t)=k\Gamma N_0 \exp(-t/\tau). \tag{9}$$

In this expression k is an instrumental constant, Γ is the radiative decay rate, $N(t)$ is the time-dependent excited-state population, N_0 is the excited-state population at time=0, and τ is the lifetime. The steady-state intensity is given by the integral of $I(t)$ over all times.

$$I=\int_0^\infty I(t)\mathrm{d}t=k\Gamma\tau N_0 \tag{10}$$

From Eqs. (5) and (6) we see that $\Gamma\tau=Q$, the quantum yield, so that the steady-state intensity is given by

$$I=kQN_0. \tag{11}$$

Now assume that the fluorophore is in two environments, 1 and 2, which display different lifetimes. The total (T) intensity observed from these two populations is given by

$$I_T(t)=kN_0[n_1\Gamma \exp(-t/\tau_1)+(1-n_1)\Gamma \exp(-t/\tau_2)], \tag{12}$$

where n_1 and $n_2=1-n_1$ are the fractional populations in each environment. This expression contains a valid but often forgotten assumption that the radiative decay rate of the fluorophore is the same in both environments. This is a good assumption for an intensity decay that is due to a single fluorophore because the radiative decay rate is determined by the extinction coefficient, which is not significantly sensitive to the local environment. For simplicity, we neglect any difference in the local refractive index surrounding the fluorophore.

We can use Eq. (13) to demonstrate that the preexponential factors in an intensity decay for a fluorophore in two environments, both without metals, represent the molecular fractions. A measured intensity decay is represented by

$$I_T(t)=\alpha_1 \exp(-t/\tau_1)+\alpha_2 \exp(-t/\tau_2), \tag{13}$$

where $\alpha_1+\alpha_2$ is typically normalized to unity. A comparison of Eqs. (13) and (14) yields the unnormalized α_1 values as

$$\alpha_1=kN_0\Gamma n_1 \tag{14}$$

and

$$\alpha_2=kN_0\Gamma(1-n_1)=kN_0\Gamma n_2. \tag{15}$$

The normalized values of α_1 and α_2 can be obtained by dividing each by the sum

$$\alpha_1+\alpha_2=kN_0\Gamma. \tag{16}$$

This yields

$$\alpha_1=n_1 \tag{17}$$

and

$$\alpha_2=n_2, \tag{18}$$

which demonstrates that the α_i values represent the molecular fractions.

The total steady-state intensities can be calculated using Eq. (10), yielding

$$I_T=kN_0[n_1Q_1+n_2Q_2]. \tag{19}$$

The fractional intensities from each environment are given by

$$f_1=\frac{n_1Q_1}{n_1Q_1+n_2Q_2} \tag{20}$$

and

$$f_2=\frac{n_2Q_2}{n_1Q_1+n_2Q_2}. \tag{21}$$

This result shows that the fractional steady-state intensities do not represent the fraction of fluorophores in each environment.

This description of a multiexponential decay may seem simple. However, this detailed description is needed to show the different meaning of the α_1 and f_i values with metal-enhanced fluorescence.

Intensity Decays with Metal-Enhanced Fluorescence

We now consider an intensity decay with metal-enhanced fluorescence. We assume there is a single fluorophore that displays a single exponential decay in the absence of metal (τ) and when near a metal (τ_m). We also assume that the metal causes an increase in the radiative decay rate from Γ in the absence of metal to Γ_m when near the metal. The total intensity decay is then given by

$$I_T(t)=kN_0[(1-m)\Gamma\exp(-t/\tau)+m\Gamma\exp(-t/\tau_m)], \tag{22}$$

where $1-m$ and m are the fractional populations distant from and near the metal, respectively. The normalized preexponential factors are thus given by

$$\alpha=\frac{(1-m)\Gamma}{(1-m)\Gamma+m\Gamma_m} \tag{23}$$

and

$$\alpha_m=\frac{m\Gamma_m}{(1-m)\Gamma+m\Gamma_m}. \tag{24}$$

In contrast to Eqs. (17) and (18), the α_1 values do not represent the molecular fractions. The change in radiative decay rate results in α_1 values that are weighted by the Γ_i values. This explains the values of α_1 summarized in Table 1. Since only a fraction of the ICG is bound to silver islands, and this fraction is probably near 25%, one does not expect the α_1 value for the short component to be larger than 0.25. However, the value for ICG-HSA on the SIF is 0.982. We believe this result is due to an increased radiative decay rate of ICG near silver, and the weighed α_m value shown in Eq. (A16).

We can use Eqs. (10) and (22) to calculate the total steady-state intensity:

$$I_T=(1-m)\Gamma\tau+m\Gamma_m\tau_m \tag{25}$$

and

$$I_T=(1-m)Q+mQ_m. \tag{26}$$

Prior to normalization, the value of I_T is proportional to the sum of the $\alpha_i\tau_i$ products, in this case m and $1-m$. For this reason we feel it is preferable to use $\langle\tau\rangle$ [Eq. (4)] rather than $\overline{\tau}$ [Eq. (3)] when comparing the changes in intensity and lifetime on quartz and near SIFs.

Acknowledgments

This work was supported by the National Institutes of Health, National Center for Research Resources (grant RR-08119) and the National Cancer Institute (grant CA-100982).

References

1. F. Schutt, J. Fischer, J. Kopitz, and F. G. Holz, ''Indocyanine green angiography in the presence of subretinal or intraretinal haemorrhages: clinical and experimental investigations,'' *Clin. Exp. Invest.* **30**(2), 110–114 (2002).
2. J. Marengo, R. A. Ucha, M. Martinez-Cartier, and J. R. Sampaolesi, ''Glaucomatous optic nerve head changes with scanning laser ophthalmoscopy,'' *Int. Ophthalmol.* **23**(4–6), 413–423 (2001).
3. H. Ishihara, H. Okawa, T. Iwakawa, N. Umegaki, T. Tsubo, and A. Matsuki, ''Does indocyanine green accurately measure plasma volume early after cardiac surgery?'' *Anesth. Analg.* **94**(4), 781–786 (2002).
4. S. G. Sakka, K. Reinhart, K. Wegscheider, and A. Meier-Hellmann, ''Comparison of cardiac output and circulatory blood volumes by transpulmonary thermo-dye dilution and transcutaneous indocyanine green measurement in critically ill patients,'' *Chest* **121**(2), 559–565 (2002).
5. P. Lanzetta, ''ICGA-guided laser photocoagulation of feeder vessels of choroidal neovascular membranes in age-related macular degeneration,'' *Retina. J. Ret. Vit. Dis.* **21**(5), 563–564 (2001).
6. J. M. Still, E. J. Law, K. G. Klavuhn, T. C. Island, and J. Z. Holtz, ''Diagnosis of burn depth using laser-induced indocyanine green fluorescence: a preliminary clinical trial,'' *Burns* **27**(4), 364–371 (2001).
7. V. M. Silva, C. Chen, G. E. Hennig, H. E. Whiteley, and J. Manautou, ''Changes in susceptibility to acetaminophen-induced liver injury by the organic anion indocyanine green,'' *Food Chem. Toxicol.* **39**(3), 271–278 (2001).
8. R. Boushel, H. Langberg, J. Olesen, M. Nowak, L. Simonsen, J. Bulow, and M. Kjaer, ''Regional blood flow during exercise in humans measured by near-infrared spectroscopy and indocyanine green,'' *J. Appl. Physiol.* **89**(5), 1868–1878 (2000).
9. K. Motomura, H. Inaji, Y. Komoike, I. Kasugai, S. Noguchi, and H. Koyama, ''Sentinel node biopsy guided by indocyanine green dye in breast cancer patients,'' *Jpn. J. Clin. Oncol.* **29**(12), 604–607 (1999).
10. V. Ntziachristos, A. G. Yodh, M. Schnall, and B. Chance, ''Concurrent MRI and diffuse optical tomography of breast after indocyanine green enhancement,'' *Proc. Natl. Acad. Sci. U.S.A.* **97**(6), 2767–2772 (2000).
11. E. M. Sevick-Muraca, G. Lopez, J. S. Reynolds, T. L. Troy, and C. L. Hutchinson, ''Fluorescence and absorption contrast mechanisms for biomedical optical imaging using frequency-domain techniques,'' *Photochem. Photobiol.* **66**(1), 55–64 (1997).
12. A. Becker, B. Riefke, B. Ebert, U. Sukowski, H. Rinneberg, W. Semmier, and K. Licha, ''Macromolecular contrast agents for optical imaging of tumors: comparison of indotricarbocyanine-labeled human serum albumin and transferrin,'' *Photochem. Photobiol.* **72**(2), 234–241 (2000).
13. J. M. Devoisselle, S. Soulie, S. Mordon, T. Desmettre, and H. Maillols, ''Fluorescence properties of indocyanine—part 1: *in-vitro* study with micelles and liposomes,'' *Proc. SPIE* **2980**, 453–460 (1997).
14. J. M. Devoisselle, S. Soulie, H. Maillols, T. Desmettre, and S. Mordon, ''Fluorescence properties of indocyanine green part 2: in vitro study related to *in vivo* behavior,'' *Proc. SPIE* **2980**, 293–302 (1997).
15. J. F. Zhou, M. P. Chin, and S. A. Schafer, ''Aggregation and degradation of indocyanine green,'' *Proc. SPIE* **2128**, 495–508 (1994).
16. R. Rajagopalan, P. Uetrecht, J. E. Bugal, S. A. Achilefu, and R. B. Dorshow, ''Stabilization of the optical tracer agent indocyanine green using noncovalent interactions,'' *Photochem. Photobiol.* **71**(3), 347–350 (2000).
17. J.-M. I. Maarek, D. P. Holschneider, and J. Harimoto, ''Fluorescence of indocyanine green in blood: intensity dependence on concentration and stabilization with sodium polyaspartate,'' *J. Photochem. Photobiol., B* **65**, 157–164 (2001).
18. J. R. Lakowicz, ''Radiative decay engineering: biophysical and biomedical applications,'' *Anal. Biochem.* **298**, 1–24 (2001).
19. J. R. Lakowicz, Y. Shen, S. D'Auria, J. Malicka, J. Fang, Z. Gryc-

zynski, and I. Gryczynski, ''Radiative decay engineering 2. effects of silver island films on fluorescence intensity, lifetimes, and resonance energy transfer,'' *Anal. Biochem.* **301**, 261–277 (2002).
20. J. R. Lakowicz, Y. Shen, Z. Gryczynski, S. D'Auria, and I. Gryczynski, ''Intrinsic fluorescence from DNA can be enhanced by metallic particles,'' *Biochem. Biophys. Res. Commun.* **286**, 875–879 (2001).
21. I. Gryczynski, J. Malicka, Y. Shen, Z. Gryczynski, and J. R. Lakowicz, ''Multiphoton excitation of fluorescence near metallic particles: enhanced and localized excitation,'' *J. Phys. Chem. B* **106**, 2191–2195 (2002).
22. J. Gersten and A. Nitzan, ''Spectroscopic properties of molecules interacting with small dielectric particles,'' *J. Chem. Phys.* **75**(3), 1139–1152 (1981).
23. D. A. Weitz and S. Garoff, ''The enhancement of Raman scattering, resonance Raman scattering, and fluorescence from molecules absorbed on a rough silver surface,'' *J. Chem. Phys.* **78**, 5324–5338 (1983).
24. J. Kummerlen, A. Leitner, H. Brunner, F. R. Aussenegg, and A. Wokaun, ''Enhanced dye fluorescence over silver island films: analysis of the distance dependence,'' *Mol. Phys.* **80**(5), 1031–1046 (1993).
25. F. Ni and T. M. Cotton, ''Chemical procedure for preparing surface-enhanced Raman scattering active silver films,'' *Anal. Chem.* **58**, 3159–3163 (1986).
26. K. Sokolov, G. Chumanov, and T. M. Cotton, ''Enhancement of molecular fluorescence near the surface of colloidal metal films,'' *Anal. Chem.* **70**, 3898–3905 (1998).
27. G. Laczko, I. Gryczynski, Z. Gryczynski, W. Wiczk, H. Malak, and J. R. Lakowicz, ''A 10-GHz frequency-domain fluorometer,'' *Rev. Sci. Instrum.* **61**, 2331–2337 (1990).
28. J. Malicka, I. Gryczynski, Z. Gryczynski, and J. R. Lakowicz, ''Effects of fluorophore-to-silver distance on the emission of cyanine-dye labeled oligonucleotides,'' *Anal. Biochem.* **315**, 57–66 (2003).
29. T. Lancaster and L. F. Stead, ''Silver acetate for smoking cessation,'' *Cochrane Database System Rev.* **2**, CD000191 (2000).
30. N. Hymowitz and H. Eckholdt, ''Effects of a 2.5 mg silver acetate lozenge on initial and long-term smoking cessation,'' *Preventive Med.* **25**(5), 537–546 (1996).
31. L. E. Bromberg, V. M. Braman, D. M. Rothstein, P. Spacciapoli, S. M. O'Conner, E. J. Nelson, D. K. Buxton, M. S. Tonetti, and P. M. Friden, ''Sustained release of silver from periodontal wafers for treatment of periodontitis,'' *J. Controlled Release* **68**(1), 63–72 (2000).
32. V. Wright, ''Oral gold for rheumatoid arthritis,'' *Br. Med. J. Clin. Res. Ed.* **289**(6449), 858–859 (1984).
33. N. Wang and X. S. Wu, ''Preparation and characterization of agarose hydrogel nanoparticles for protein and peptide drug delivery,'' *Pharmaceuti. Dev. Technol.* **2**(2), 135–142 (1997).
34. J. D. Hood, M. Bednarski, R. Frausto, S. Guccione, R. A. Reisfeld, R. Xiang, and D. A. Cheresch, ''Tumor regression by targeted gene delivery to the neovasculature,'' *Science (Washington, DC, U.S.)* **296**, 2404–2407 (2002).
35. K. Adzamli, R. B. Dorshow, M. R. Hynes, D. Li, D. L. Nosco, and M. D. Adams, ''Preliminary evaluation of a polyethyleneglycol-stabilized manganese-substituted hydroxylapatite as an intravascular contrast agent for MR angiography,'' *J. Magn. Reson. Imag.* **7**(1), 204–208 (1997).
36. L. Josephson, E. V. Groman, E. Menz, J. M. Lewis, and H. Bengele, ''A functionalized superparamagnetic iron oxide colloid as a receptor directed MR contrast agent,'' *Magn. Reson. Imaging* **8**, 637–646 (1990).
37. J. Yguerabide and E. E. Yguerabide, ''Light-scattering submicroscopic particles as highly fluorescent analogs and their use as tracer labels in clincal and biological applications, 1. theory,'' *Anal. Biochem.* **262**, 137–156 (1998).
38. J. Yguerabide and E. E. Yguerabide, ''Light-scattering submicroscopic particles as highly fluorescent analogs and their use as tracer labels in clincal and biological applications 2. experimental characterization,'' *Anal. Biochem.* **262**, 157–176 (1998).
39. S. Schultz, D. R. Smith, J. J. Mock, and D. A. Schultz, ''Single-target molecule detection with nonbleaching multicolor optical immunolabels,'' *Proc. Natl. Acad. Sci. U.S.A.* **97**(3), 996–1001 (2000).